PAPER

Check for updates

Electron-correlation driven structural instability and adsorption mechanism in the metal–organic framework NU2100

W. Graham, [ID] [ab] T. Jenkins,[ab] C. Fivecoat,[ab] J. H. West,[bc] E. C. Hill,[bc] Y. Zeng,[bc] S. Ullah [ID] [ab] and T. Thonhauser [ID] *[ab]

Metal–organic frameworks have garnered considerable interest due to their high porosity, large surface areas, and often easy synthesis, offering a vast structural diversity of interest to wide-ranging applications. Recently, the novel structure NU2100 showed notable selectivity of CO_2 and H_2 compared to C_2H_4 and C_2H_6, a promising step towards integrated carbon capture and utilization. Here, we investigate NU2100 using *ab initio* techniques to understand the mechanism of adsorption observed experimentally. Our calculations uncover a surprising structural instability—associated with the strongly correlated Cu(I) sites—that drives a gate-opening effect. This structural instability has significant implications for the binding affinity and diffusion barriers of the guest molecules in NU2100. The thermodynamic, kinetic, and structural stability insights provided by our calculations lead to a complete mechanistic understanding of the adsorption behavior in NU2100 observed experimentally.

1 Introduction

Metal–organic frameworks (MOFs) have emerged as a transformative class of materials, captivating the materials science community with their structural diversity and multifunctionality.[1–4] These crystalline solids, constructed from metal clusters bridged by organic linkers, combine exceptional porosity and tunability with relative ease of synthesis, making them promising candidates for applications ranging from gas storage and separation to catalysis and sensing.[5–10] Copper-based MOFs have attracted special attention, owing to their unique electronic properties and reactivity.[11–13] However, the stability of such frameworks under ambient conditions remains a significant challenge, particularly for those with open-metal sites.[14,15] In this context, the recently developed NU2100 is noteworthy because it maintains ambient stability despite featuring an open Cu(I) site—which are typically prone to rapid oxidation.[16] Recent experimental results for NU2100 reveal exceptional selectivity for CO_2 over various gases, as well as promising uptake and recyclability in the presence of H_2O.[17] Capturing CO_2 emissions from industrial processes and power plants is essential, and achieving efficient, cost-effective separation under ambient conditions is vital for widespread adoption of carbon capture and storage technologies.

Size exclusion was hypothesized by Sengupta *et al.* to be the mechanism that explains the extremely low uptake of C_2H_4 and C_2H_6 in NU2100,[17] while easily up-taking CO_2 and H_2O. However, frameworks of similar pore size have been shown to uptake the same and even larger guest molecules.[18–22] Thus, to test the hypothesis of size exclusion, we turned to *ab initio* calculations to gain a comprehensive picture of NU2100's enticing properties. Specifically, we investigated the adsorption behavior of five key adsorbates: H_2O, CO_2, C_2H_4, C_2H_6, and C_2H_2. The inclusion of acetylene (C_2H_2), a linear molecule analogous to CO_2, is motivated by the need to clarify the role of molecular geometry in adsorption. Upon investigation, we uncovered a structural instability in NU2100 due to the inclusion of Hubbard U corrections for the copper sites, see Fig. 1. Our *ab initio* calculations suggest that the more collapsed ground state for NU2100 leads to kinetics being the dominant mechanism in the observed adsorption phenomena. These findings provide a refined mechanistic understanding of gas uptake in this Cu-based MOF and offer insights that may guide the design of future frameworks optimized for gas storage and separation applications.

2 Methods

Electronic structure calculations were conducted utilizing the Vienna *Ab initio* Simulation Package (VASP),[23,24] a software for *ab initio* simulations based on density functional theory (DFT). For our simulations we used a structure with two pores per unit cell (with 128 atoms), see Fig. 1. This unit cell was chosen instead of the primitive cell in order to be consistent with ref. 16 and because it allows for the study of lower loading

[a]Department of Physics, Wake Forest University, Winston Salem, NC 27109, USA. E-mail: thonhauser@wfu.edu

[b]Center for Functional Materials, Wake Forest University, Winston Salem, NC 27109, USA

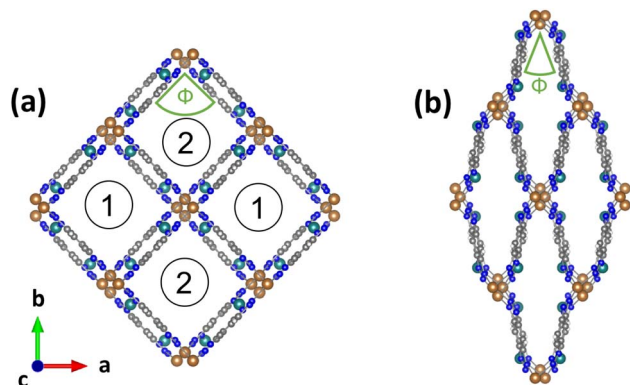*[c]Department of Chemistry, Wake Forest University, Winston Salem, NC 27109, USA*

This journal is © The Royal Society of Chemistry 2025

J. Mater. Chem. A, 2025, **13**, 30661–30668 | 30661

Fig. 1 (a) Open-pore structure of NU2100 with $\Phi = 90°$. (b) Collapsed-pore structure of NU2100 with $\Phi = 50°$. The structure contains Cu atoms in two different coordinations, *i.e.* open copper sites (depicted in turquoise color) and fully saturated copper sites (depicted in golden color); the latter are structurally more relevant. Note that both images depict two unit cells, and each unit cell consists of two chemically equivalent pores labeled 1 and 2. The cell parameters can be found in Table S1. Carbon atoms are represented in gray, nitrogen in blue, and hydrogen in white.

concentrations—showcasing preferential binding order. The maximum energy plane-wave cutoff for the basis was set to 600 eV, and the precision of the total energy convergence for the self-consistency loop was set to 10^{-6} eV. Structural optimization was considered achieved when the forces on each atom were at or below 5 meV Å^{-1}. The Brillouin zone was sampled on a $2 \times 2 \times 1$ grid centered at the Γ point. The van der Waals density functional vdW-DF1 (ref. 25–28) was employed to account for the subtle but critical dispersion interactions that are essential to capture the adsorption behavior in this system. The inclusion of a Hubbard $U^{29,30}$ correction is especially important for NU2100, where the Cu(I) transition metal centers play a significant role in electron localization, which heavily impact the electronic properties. Rather than relying on generic U values,[31] we determined the U values for the two different coordination environments self-consistently using a linear-response method.[32] This self-consistent approach ensures that the U values reflect the specific electronic environment around each Cu center, adapting to the coordination and oxidation state of the metal.

To characterize the thermodynamic behavior, optimal binding locations were found by creating 100 initial configurations using a simple Monte Carlo approach, ensuring unique configurations that adequately sample the pore. The geometries were then relaxed, optimizing atomic positions and unit-cell parameters. The incremental binding energies were found by taking the total energy of the MOF framework with n adsorbed guest molecules and subtracting the sum of the total energies of the gas-phase guest molecule and the framework with $n - 1$ guest molecules, *i.e.*

$$E_b(n) = E_{n \text{ guests+MOF}} - E_{\text{guest}} - E_{(n-1) \text{ guests+MOF}} \quad (1)$$

A similar process produces the induced charge density plots, except charge density is used instead of total energy.

To compute diffusion barriers, we employed the climbing-image nudged elastic band (CI-NEB) method in conjunction with variable-cell optimizations, which better capture the structural response of the flexible NU2100 framework.[33,34] Due to the combination of these algorithms, convergence of these CI-NEB calculations proved challenging. To ensure full convergence of all diffusion pathways, we had to loosen the stringent maximum force threshold of 0.005 eV Å^{-1} to a slightly looser criterion of 0.02 eV Å^{-1} for all our CI-NEB calculations.

To investigate the structural bistability of NU2100 and capture the double-well nature of its energy landscape, we systematically varied the length of the a-axis while allowing the remaining lattice vectors and atomic positions to relax. This method provides a convenient way to control the Φ angle in Fig. 1 and enables an accurate tracing of the total energy profile as a function of pore dimension, revealing distinct minima corresponding to the closed-pore configurations. This approach is well suited to flexible framework materials, where the structural reorganization along a specific axis can be decoupled from relaxation in the orthogonal directions. The Φ angle is calculated by simply multiplying the arctangent of the ratio of the a-axis to b-axis by two.

Lastly, due to the high degree of structural flexibility, careful attention was given to the Pulay stress effects during all structural relaxations.[35,36] To mitigate Pulay stress, we first performed static calculations of the structure at our standard plane-wave cutoff and at a cutoff twice as large (1200 eV). The Pulay stress was then computed as the difference between the external pressures obtained at the two different cutoffs values. The structure was then relaxed using this corrective Pulay stress. Although our calculated value for the Pulay correction was only $\sim$−2.2 kBar, it had noticeable effects due to the softness of NU2100.

3 Results

3.1. Structural instability driven by on-site interaction

The inclusion of self-consistent Hubbard U corrections in our DFT calculations fundamentally alters the predicted equilibrium structure of NU2100. Standard DFT (*i.e.*, $U = 0$ eV) favors a more open-pore geometry with $\Phi \approx 80.3°$, intriguingly close to the experimental value of $\Phi \approx 81.8°$.[16] However, with such a widely open pore it is difficult to argue for the originally proposed size exclusion of C_2H_4 and C_2H_6,[17] when other frameworks of similar pore size easily uptake the same and even larger guest molecules.[18–22] We find the answer by going beyond standard DFT—upon introduction of our self-consistently calculated U values of 7.0 eV and 7.9 eV for the open and saturated copper sites, the structure undergoes a contraction, yielding a closed-pore configuration with a significantly reduced Φ angle (Fig. 1b). This collapse is not a subtle deformation, but rather a qualitative shift in equilibrium geometry. As shown in Fig. 2, the total energy profile exhibits a distinct double-well potential as a function of Φ, with the minimum favoring a collapsed configuration, see Table S1.

This bistability is a direct consequence of electronic correlation effects, captured through our linear-response derived U values. While modest U values already introduce significant structural softening (see *e.g.*, $U = 4$ eV, typical for Cu oxides,[31] in
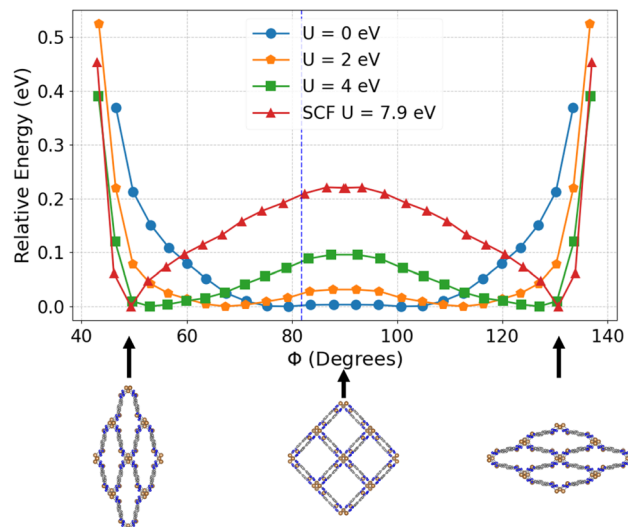
Fig. 2 Double-well potential of empty NU2100 as a function of Hubbard U, favoring a more collapsed structure for higher U values. The actual value used in all calculations was $U = 7.9$ eV for the saturated copper site and $U = 7.0$ eV for the open site. The structures below represent the corresponding configurations of NU2100. The blue dashed line indicates the experimental structure. Φ is defined in Fig. 1. The stark increase in energy below 50° and above 130° is dictated by steric hindrance of the fully collapsed structure and thus is nearly independent of U.

Fig. 3 Charge redistribution when going from $U = 0$ eV to $U = 7.9$ eV. (a) View of the saturated metal site, where the charge localizes from a tetrahedral conformation into a more spherical configuration around the copper sites when U is introduced, removing the scaffold to support the open structure. (b) View of the open metal site, where the charge rearrangement has little effect on the structure. Regions depicted in yellow indicate on-site charge accumulation. Conversely, blue regions show the associated charge depletion. The iso-value is drawn at 0.0015 e Å^{-3}.

Fig. 2), the fully self-consistent U values derived for NU2100's unique Cu environments intensify this behavior. Relatively large U values, especially in nitrogen coordinated environments, are not unusual for copper and have been reported for several situations.[37–40] We emphasize that it is the U on the fully saturated copper sites—located at the tetrahedral vertices of the framework—that drives this collapse. The U on the open Cu sites has negligible structural influence, as confirmed by calculations isolating the open site (see Fig. S13).

The mechanism of collapse can be understood by examining the induced charge redistribution between $U = 0$ and $U = 7.9$ eV. As shown in Fig. 3a, the electron density in the open-pore configuration is delocalized in a tetrahedral arrangement around the saturated Cu atoms, providing a stabilizing scaffold that supports the expanded geometry. When U is applied, this density localizes into a more compact, spherically symmetric state centered on the Cu sites. The loss of the tetrahedral charge support scaffold leads to mechanical instability and collapse. This localization is typical of correlation-driven behavior: U penalizes partial orbital occupation, driving electrons toward atomic-like localization. In the context of NU2100, this localization energetically favors a collapsed structure with $\Phi \approx 50°$, in contrast to the 90° angle seen in the completely open-pore state. The open Cu sites also exhibit charge redistribution (Fig. 3b), but this has little structural consequence (Fig. S13) since the open sites are within the linker and they do not support a charge-delocalized framework backbone in the same way the saturated sites do. As a result, the U correction on these sites shifts electronic density without driving mechanical deformation.
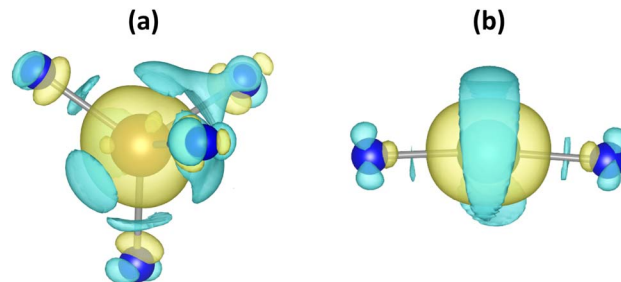
This correlation-induced structural bistability is more than a theoretical curiosity. It has direct implications for adsorption: the collapsed structure introduces a gate-opening barrier that guests must overcome to enter the pore. The experimental structure reported with $\Phi \approx 81.8°$ likely represents a partially opened, solvent-containing state.[16] We support this statement with explicit calculations for NU2100 containing dimethylformamide (DMF) solvent molecules in the next section. In the fully activated form, as modeled here, the framework prefers a more collapsed geometry unless guest-induced opening is triggered. Our results suggest that low-temperature PXRD on a fully activated sample could reveal the more collapsed form predicted by theory. At elevated temperatures accessed during experiments, the framework samples a broader range of Φ angles, making transitions to more open-pore states more probable due to thermal activation. Additionally, we find that an uniaxial pressure of ~0.53 kBar can drive the closed-pore structure into the open-pore state (Fig. S15).

Lastly, we studied the effects of the on-site Hubbard U value on the binding energy directly, decoupling it from structural aspects. We selectively varied the U value on the open metal sites from 0 to 7.0 eV, while keeping the saturated site fixed at $U = 7.9$ eV. This selective variation is justified as (i) guest molecules primarily interact near the open Cu centers rather than the saturated sites, and (ii) our calculations confirm minimal structural distortion from variations in open-site U value (Fig. S13). Our calculations reveal a small reduction in binding energy for the various guest molecules, *i.e.* approximately 9%, when going from $U = 0$ eV to $U = 7.0$ eV. This reduction indicates that increasing the U value at the open copper sites slightly weakens the local guest–framework interactions, independent of larger-scale structural rearrangements, further highlighting the nuanced role of electron localization effects on the adsorption characteristics of NU2100.

This journal is © The Royal Society of Chemistry 2025

J. Mater. Chem. A, 2025, **13**, 30661–30668 | **30663**

Table 1 Incremental binding energies $E_b(n)$ (in eV) from eqn (1) of various guest molecules as a function of the number n of molecules adsorbed per unit cell. Numbers in brackets indicate the pore (1 or 2, defined in Fig. 1) to which the incremental guest molecules bind most favorably. This explicitly reveals whether subsequent molecules prefer occupying the same pore or migrating to the second pore

Guest	$n = 1$	$n = 2$	$n = 3$	$n = 4$
H_2O	−0.473 [1]	−0.586 [1]	−0.493 [1]	−0.713 [1]
CO_2	−0.558 [1]	−0.588 [2]	−0.599 [1]	−0.600 [2]
C_2H_2	−0.486 [1]	−0.543 [1]	−0.550 [2]	−0.561 [2]
C_2H_4	−0.511 [1]	−0.601 [1]	−0.609 [2]	−0.624 [2]
C_2H_6	−0.603 [1]	−0.690 [1]	−0.700 [2]	−0.714 [2]

3.2. Adsorption

Regarding adsorption phenomena, our calculations reveal a binding affinity order of $C_2H_6 > CO_2 > C_2H_4 > C_2H_2 > H_2O$ for single-molecule interactions (see Table 1 for $n = 1$). This thermodynamic hierarchy, however, does not match the experimental uptake behavior observed by Sengupta *et al.*,[16] where only CO_2 and H_2O exhibit appreciable adsorption, and C_2H_6 and C_2H_4 show negligible uptake. This mismatch underscores that binding energy alone does not control adsorption in NU2100—kinetic and structural constraints must also be considered.

To understand this further, we first examined the binding environments of each guest. We find that each guest type binds in the vicinity of one of four chemically identical locations within the unit cell—a sort of universal binding site. As visualized in the SI (Fig. S1 and S2), CO_2 preferentially binds with the linker atoms rather in close proximity to the open metal site. The carbon center of CO_2 forms favorable interactions with the linker nitrogen atoms, while the oxygen atoms interact with nearby hydrogen and carbon atoms of the linker. This occurs consistently across all four CO_2 configurations, which populate the two chemically identical adsorption sites in both symmetry-equivalent pores, with relatively little guest–guest interaction and no significant deviation in charge redistribution pattern. Interestingly, CO_2 is the only guest molecule that prefers to bind in the adjacent pore for $n = 2$. This is another indicator of the weak guest–guest interaction for CO_2 in this particular confined environment. It should also be noted that, eventually, the incremental binding energy will become unfavorable as the number of guest molecules increases. However, we did not go beyond $n = 4$ in our study because (i) the experimental uptake for CO_2 is limited to about 3–4 guests per unit cell while C_2H_4 and C_2H_6 show no appreciable uptake,[16] and (ii) the configurational space grows exponentially.

In contrast, H_2O shows both framework binding and strong guest–guest interaction. The first two water molecules, due to their small size, both bind in the vicinity of one of the distinct linker site observed to be the primary binding cite across each molecule. They form hydrogen bonds with nitrogen atoms of the linker and the oxygen interacts with the carbon and hydrogen sites on the linker (Fig. S3 and S4). Interestingly, we observe a noticeable reduction in incremental binding energy at

$n = 3$ (from −0.586 eV at $n = 2$ to −0.493 eV at $n = 3$, see Table 1), indicative of the changing nature of the water clustering environment. Physically, this reduction results from the $n = 3$ molecule preferring to bind to the equivalent optimal binding site in the same pore rather than continuing the chain (Fig. S5). Evaluating incremental binding energies per additional framework hydrogen bond formed provides further insight: the addition of the second water molecule yields approximately 0.178 eV for the single hydrogen bond formed, while the third molecule contributes only about 0.057 eV as it primarily binds with the framework. This intermediate drop is recovered at $n = 4$, with the incremental binding energy significantly increasing again yielding an average of 0.232 eV for the two framework hydrogen bonds formed. This is consistent with previous studies of H_2O frameworks.[41–43]
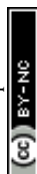
The fourth water molecule binds between the second and the third, forming a continuous hydrogen-bonded chain (Fig. S6). This is intriguing as water is the only molecule we studied that exhibits preference to build large guest–guest frameworks in the same pore rather than to bind at the universal primary binding site. This cooperative interaction is well-documented in confined environments and accounts for the observed strengthening of incremental binding with increasing loading—a hallmark of water cluster formation.[9,44]

C_2H_2 binds differently still. Fig. S7 and S8 show it interacts directly with the open copper site *via* the carbon atom, while the hydrogens interact with linker nitrogens. The strong interaction with the open metal site is likely driven by the spatially extended triple bond. It fills the first pore with two molecules before occupying the second, and unlike H_2O, does not benefit much from cooperative guest–guest interactions at this loading level.

For C_2H_4 and C_2H_6 (Fig. S9–S12), the binding also initially targets linker atoms and occasionally the open metal site. Guest–guest interactions are minimal even at higher loadings. The third and fourth C_2H_4 and C_2H_6 molecules still exhibit favorable binding energies and move into the second pore. However, this thermodynamic preference is not realized experimentally due to the kinetic constraints discussed below.

3.3. Gate opening

The experimental framework likely exists in a collapsed or partially collapsed state at ambient conditions, destabilized by correlation-driven localization effects (see Fig. 1b). For adsorption to occur, the structure must undergo a gate-opening conformational change. This transformation requires a structural fluctuation to a more open-pore geometry. We now investigate how the pore opens up as a function of loading of the guest molecules. Results are depicted in Fig. 4, where it can be seen that larger molecules require a significantly larger pore opening to be accommodated. The stagnation in Φ at intermediate loadings arises from asymmetric guest distributions across the two symmetry-equivalent pores, with *e.g.* two guests in one pore *vs.* one in the other. Another noticeable increase in Φ would occur at $n = 5$. Based on our analysis in Fig. 2 and 4, the degree of opening required to accommodate one C_2H_4 or C_2H_6 corresponds to a deformation energy of ∼100 meV, roughly four

30664 | *J. Mater. Chem. A*, 2025, **13**, 30661–30668

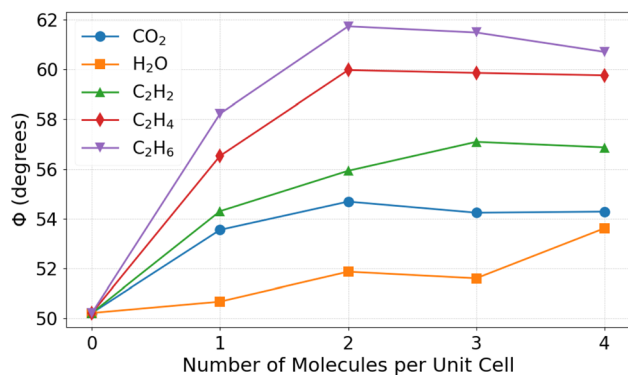This journal is © The Royal Society of Chemistry 2025

Fig. 4 Pore opening upon introduction of up to four guest molecules per unit cell. Φ is the angle defined in Fig. 1. As expected, larger molecules require a significantly larger pore opening to be accommodated. Note that molecules are accommodated in the two pores as indicated by their preference in Table 1.

Table 2 Diffusion energy barriers (in eV) for guest molecules moving along the primary diffusion pathway within NU2100. Barriers are reported for diffusion of one molecule through an empty pore ($n = 1$) and a pore pre-loaded with another molecule of the same kind ($n = 2$). Pre-adsorbed molecules significantly influence subsequent diffusion by raising kinetic barriers

Guest	$n = 1$	$n = 2$
H_2O	0.103	0.188
CO_2	0.086	0.356
C_2H_2	0.023	0.625
C_2H_4	0.036	0.466
C_2H_6	0.076	0.595

times the thermal energy at room temperature. While this barrier is not large, it is important to consider as larger molecules experience an additional structural opening barrier that must also be taken into account when analyzing diffusion barriers in the following section. Small guests such as CO_2 and H_2O, in contrast, require only minor pore expansion with barriers of ~50 meV, facilitating frequent adsorption events which aids in the higher uptake.

Additionally, we find that even a single C_2H_6 molecule significantly increases the gate-opening barrier due to its interaction with the framework. Upon adsorption, C_2H_6 acts as a dispersive "bridge" or "strut", simultaneously interacting with opposite sides of the pore *via* van der Waals forces, see Fig. S11. For the framework to undergo its characteristic opening deformation, one of these interactions must be broken, introducing an additional energetic penalty. This added resistance contributes to the overall increase in the double-well barrier height (see Fig. S14) and explains why even initial adsorption events of C_2H_6 can kinetically trap the framework in a collapsed or partially collapsed state, effectively bottlenecking the system.

In addition to the molecules considered in Fig. 4, we have also studied the pore opening upon inclusion of DMF, *i.e.* the solvent used during synthesis of NU2100. Importantly, our hypothesis regarding the solvent-induced intermediate structure is supported as we find $\Phi \approx 80.8°$ for three DMF per pore, strikingly close to the experimental measurement of 81.8°.[16] This loading amount also coincides with where the incremental binding becomes unfavorable. This agreement suggests that the experimentally observed intermediate structure results from solvent stabilization, whereby DMF molecules effectively mitigate the electron-correlation driven structural collapse. Consequently, the experimentally reported angle may not represent the intrinsic structure of fully activated NU2100 but rather a solvent-stabilized intermediate. Such solvent-induced structural stabilization phenomena have precedence in other flexible MOF systems and highlight the critical role solvent molecules can play in determining observed MOF geometries under experimental conditions.[45,46]

3.4. Kinetics of adsorption

To elucidate kinetic factors governing uptake in NU2100, we calculated the diffusion energy barriers for each adsorbate at different loading levels using a transition-state search algorithm. The results are shown in Table 2. These barriers represent the minimum-energy path for a molecule to diffuse from the primary binding site in one unit cell to the same site in the next unit cell along the one-dimensional pore channel. For CO_2, the diffusion barrier remains moderate for single and double molecule loading, ranging from 0.086 eV to 0.356 eV. H_2O exhibits improved kinetics, starting at 0.103 eV and rising to only 0.188 eV. By contrast, C_2H_4 and C_2H_6 display a distinct kinetic profile. At single molecule loading, the diffusion barriers are comparable to CO_2 (0.036 and 0.076 eV), but they rise steeply upon the addition of another guest molecule. At $n = 2$, the barriers for C_2H_4 and C_2H_6 exceed 0.466 and 0.595 eV, respectively. These large barriers suppress continued diffusion, effectively bottlenecking the system. Once a molecule is adsorbed near the surface, further migration of additional molecules into the pore becomes highly unlikely. C_2H_2, despite being a small hydrocarbon, exhibits a similar behavior to C_2H_4 and C_2H_6. This is due to its strong, directional binding to the open Cu sites and linker nitrogens (Fig. S7 and S8), which effectively immobilizes it and makes diffusion energetically costly under bimolecular loading. This implies that C_2H_2 would have low loading at room temperature.

Diffusion rates are governed by the Arrhenius equation. Assuming a relatively constant pre-exponential factor across the various guest molecules, their relative diffusion times between species can be estimated using the exponential difference in activation energies. For instance, at $n = 2$, the effective diffusion time for C_2H_6 compared to CO_2 is approximately:

$$\frac{t_{C_2H_6}}{t_{CO_2}} \sim e^{0.239 \text{ eV}/k_B T} \approx 1.4 \times 10^4, \quad (2)$$

indicating that C_2H_6 would require four orders of magnitude longer to diffuse than CO_2. This kinetic delay provides a compelling explanation for the near-zero uptake of C_2H_6 and C_2H_4 reported in experiment,[17] despite their strong thermodynamic binding affinity in Table 1. The significant rise in diffusion barrier with loading suggests the possibility of kinetic jamming. That is, once a few large guest molecules occupy the

surface, they prevent subsequent molecules from diffusing further, effectively sealing off the interior. This mechanism has been studied in related systems, where dynamic bottlenecking inhibits pore access.[47–50] In NU2100, our data supports this behavior, as the presence of even a single C_2H_6 or C_2H_4 molecule raises the barrier for the next significantly.

The effect is further compounded by the gate-opening requirement. As discussed above, the structure must fluctuate into a more open geometry ($\Phi > 60°$) to permit entry of larger guests. Although this structural fluctuation requires relatively modest additional energy (≈ 100 meV), it remains less frequent than smaller structural adjustments needed for the other guests. Hence, adsorption is both thermodynamically favorable and kinetically improbable—the defining feature of gate-controlled selectivity. Taken together, these results confirm that diffusion in NU2100 is strongly guest-dependent and dynamically constrained. The interplay of the two barrier effects produces a highly selective adsorption profile that is not apparent from thermodynamic data alone and explains the experimental evidence from ref. 17: CO_2 and H_2O can easily diffuse and adsorb in NU2100, while C_2H_4 and C_2H_6 are kinetically excluded.

4 Conclusion

We have uncovered a correlation-driven structural instability in NU2100 that governs its guest selectivity and adsorption behavior. Using *ab initio* calculations we demonstrate that electron localization destabilizes the open-pore structure and drives a collapse into a narrow-pore configuration. This behavior gives rise to a bistable energy landscape that couples electronic and mechanical degrees of freedom. Adsorption is thus controlled not by thermodynamics alone, but also by a combination of a gate-opening transition and kinetics. Smaller molecules such as CO_2 and H_2O can enter the framework with only modest structural deformation and diffusion barriers, enabling adsorption. In contrast, larger hydrocarbons like C_2H_4 and C_2H_6 require energetically unfavorable expansions to enter the framework and also experience a sharp increase in diffusion barriers with loading, effectively excluding those molecules. While NU2100's exclusion of larger hydrocarbons appears to resemble conventional size exclusion, our findings reveal it to be more nuanced. It is not solely due to static pore size, but rather an interplay between a gate-opening mechanism and the unique kinetic barriers for each molecule. This distinction is highlighted by C_2H_2's kinetic exclusion, despite its similar size to CO_2, clarifying the role of linear geometry and the limits of purely size-based arguments.

Our findings underscore the importance of treating electronic correlation when modeling MOFs with transition-metal sites. The framework's response to electronic and chemical stimuli plays a defining role in selectivity—a principle that may be harnessed in the design of next-generation materials for carbon capture and separation, especially under humid or ambient conditions. More broadly, NU2100 exemplifies how gate-opening behavior can be engineered by tuning flexibility through choice of transition metal nodes, offering a path forward for highly selective, robust carbon capture frameworks.

Author contributions

W. Graham: conceptualization (equal); formal analysis (lead); investigation (lead); writing – review & editing (equal). T. Jenkins: investigation (supporting). C. Fivecoat: investigation (supporting). J. H. West: investigation (supporting). E. C. Hill: investigation (supporting). Y. Zeng: investigation (supporting). S. Ullah: conceptualization (equal); writing – review & editing (supporting). T. Thonhauser: conceptualization (equal); supervision (lead); writing – review & editing (equal); funding acquisition (lead); resources (lead).

Conflicts of interest

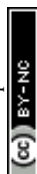The authors declare no conflicts of interest.

Data availability

The data supporting this article have been included as part of the SI. See DOI: **https://doi.org/10.1039/d5ta05367f**.

Acknowledgements

References

1 H. K. Chae, D. Y. Siberio-Pérez, J. Kim, Y. Go, M. Eddaoudi, A. J. Matzger, M. O'Keeffe and O. M. Yaghi, A route to high surface area, porosity and inclusion of large molecules in crystals, *Nature*, 2004, **427**, 523.

2 O. K. Farha and J. T. Hupp, Rational Design, Synthesis, Purification, and Activation of Metal-Organic Framework Materials, *Acc. Chem. Res.*, 2010, **43**, 1166.

3 O. M. Yaghi, M. O'Keeffe, N. W. Ockwig, H. K. Chae, M. Eddaoudi and J. Kim, Reticular synthesis and the design of new materials, *Nature*, 2003, **423**, 705.

4 H. Furukawa, K. E. Cordova, M. O'Keeffe and O. M. Yaghi, The Chemistry and Applications of Metal-Organic Frameworks, *Science*, 2013, **341**, 1166.

5 P. Horcajada, T. Chalati, C. Serre, B. Gillet, C. Sebrie, T. Baati, J. F. Eubank, D. Heurtaux, P. Clayette, C. Kreuz, J.-S. Chang, Y. K. Hwang, V. Marsaud, P.-N. Bories, L. Cynober, S. Gil, G. Férey, P. Couvreur and R. Gref, Porous metal-organic-framework nanoscale carriers as a potential platform for drug delivery and imaging, *Nat. Mater.*, 2010, **9**, 172.

6 J. Lee, O. K. Farha, J. Roberts, K. A. Scheidt, S. T. Nguyen and J. T. Hupp, Metal-organic framework materials as catalysts, *Chem. Soc. Rev.*, 2009, **38**, 1450.

30666 | *J. Mater. Chem. A*, 2025, **13**, 30661–30668

This journal is © The Royal Society of Chemistry 2025

7 W. P. Lustig and J. Li, Luminescent metal-organic frameworks and coordination polymers as alternative phosphors for energy efficient lighting devices, *Coord. Chem. Rev.*, 2018, **373**, 116.

8 X. Zhao, Y. Wang, D.-S. Li, X. Bu and P. Feng, Metal-Organic Frameworks for Separation, *Adv. Mater.*, 2018, **30**, 1705189.

9 K. Tan, S. Ullah, H. Pandey, E. M. Cedeño-Morales, H. Wang, K. Wang, H.-C. Zhou, J. Li and T. Thonhauser, Competitive Adsorption of NH_3 and H_2O in Metal-Organic Framework Materials: MOF-74, *Chem. Mater.*, 2022, **34**, 7906.

10 J. Liu, J. Miao, S. Ullah, K. Zhou, L. Yu, H. Wang, Y. Wang, T. Thonhauser and J. Li, A Water-Resistant Hydrogen-Bonded Organic Framework for Ethane/Ethylene Separation in Humid Environments, *ACS Mater. Lett.*, 2022, **4**, 1227.

11 L. S. Xie, G. Skorupskii and M. Dincă, Electrically Conductive Metal-Organic Frameworks, *Chem. Rev.*, 2020, **120**, 8536.

12 U. Nwosu and S. Siahrostami, Copper-based metal-organic frameworks for CO_2 reduction: selectivity trends, design paradigms, and perspectives, *Catal. Sci. Technol.*, 2023, **13**, 3740.

13 S. M. S. Islam, R. Yasmeen, G. Verma, S. M. Tekarli, V. N. Nesterov, S. Ma and M. A. Omary, A Copper-Based Metal-Organic Framework for Selective Separation of C_2 Hydrocarbons from Methane at Ambient Conditions: Experiment and Simulation, *Inorg. Chem.*, 2024, **63**, 8664.

14 N. K. Gupta, E. J. Kim, J. Bae and K. S. Kim, Probing the origin and stability of bivalency in copper based porous coordination network and its application for H_2S gas capture, *Sci. Rep.*, 2022, **12**, 15388.

15 Z. Jiang, Y. Zou, T. Xu, L. Fan, P. Zhou and Y. He, A hydrostable cage-based MOF with open metal sites and Lewis basic sites immobilized in the pore surface for efficient separation and purification of natural gas and C_2H_2, *Dalton Trans.*, 2020, **49**, 3553.

16 D. Sengupta, P. Melix, S. Bose, J. Duncan, X. Wang, M. R. Mian, K. O. Kirlikovali, F. Joodaki, T. Islamoglu, T. Yildirim, R. Q. Snurr and O. K. Farha, Air-Stable Cu(I) Metal-Organic Framework for Hydrogen Storage, *J. Am. Chem. Soc.*, 2023, **145**, 20492.

17 D. Sengupta, S. Bose, X. Wang, N. M. Schweitzer, C. D. Malliakas, H. Xie, J. Duncan, K. O. Kirlikovali, T. Yildirim and O. K. Farha, Integrated CO_2 Capture and Conversion by a Robust Cu(I)-Based Metal-Organic Framework, *J. Am. Chem. Soc.*, 2024, **146**, 27006.

18 H. Wang, X. Dong, E. Velasco, D. H. Olson, Y. Han and J. Li, One-of-a-kind: a microporous metal-organic framework capable of adsorptive separation of linear, mono- and di-branched alkane isomers *via* temperature- and adsorbate-dependent molecular sieving, *Energy Environ. Sci.*, 2018, **11**, 1226.

19 F. Xie, J. Liu, W. Graham, S. Ullah, E. M. C. Morales, K. Tan, T. Thonhauser, H. Wang and J. Li, The effect of pore structure in ethane-selective metal-organic frameworks for ethylene purification, *Chem. Eng. J.*, 2023, **473**, 145096.

20 P. Guo, Y. Ying, M. Chang and D. Liu, One ethane-selective metal-organic framework with customized pore size and specific binding sites for efficient purification of ethylene, *Sep. Purif. Technol.*, 2023, **323**, 124465.

21 M. Zhou and J. Wu, Inverse design of metal-organic frameworks for C_2H_4/C_2H_6 separation, *npj Comput. Mater.*, 2022, **8**, 256.

22 J. Pei, J.-X. Wang, K. Shao, Y. Yang, Y. Cui, H. Wu, W. Zhou, B. Li and G. Qian, Engineering microporous ethane-trapping metal-organic frameworks for boosting ethane/ethylene separation, *J. Mater. Chem. A*, 2020, **8**, 3613.

23 G. Kresse and J. Furthmüller, Efficient iterative schemes for emphab initio total-energy calculations using a plane-wave basis set, *Phys. Rev. B: Condens. Matter Mater. Phys.*, 1996, **54**, 11169.

24 G. Kresse and D. Joubert, From ultrasoft pseudopotentials to the projector augmented-wave method, *Phys. Rev. B: Condens. Matter Mater. Phys.*, 1999, **59**, 1758.

25 M. Dion, H. Rydberg, E. Schröder, D. C. Langreth and B. I. Lundqvist, Van der Waals Density Functional for General Geometries, *Phys. Rev. Lett.*, 2004, **92**, 246401.

26 T. Thonhauser, V. R. Cooper, S. Li, A. Puzder, P. Hyldgaard and D. C. Langreth, Van der Waals density functional: Self-consistent potential and the nature of the van der Waals bond, *Phys. Rev. B: Condens. Matter Mater. Phys.*, 2007, **76**, 125112.

27 K. Berland, V. R. Cooper, K. Lee, E. Schröder, T. Thonhauser, P. Hyldgaard and B. I. Lundqvist, van der Waals forces in density functional theory: a review of the vdW-DF method, *Rep. Prog. Phys.*, 2015, **78**, 066501.

28 T. Thonhauser, S. Zuluaga, C. A. Arter, K. Berland, E. Schröder and P. Hyldgaard, Spin Signature of Nonlocal Correlation Binding in Metal-Organic Frameworks, *Phys. Rev. Lett.*, 2015, **115**, 136402.

29 V. I. Anisimov, J. Zaanen and O. K. Andersen, Band theory and Mott insulators: Hubbard *U* instead of Stoner *I*, *Phys. Rev. B: Condens. Matter Mater. Phys.*, 1991, **44**, 943.

30 S. L. Dudarev, G. A. Botton, S. Y. Savrasov, C. J. Humphreys and A. P. Sutton, Electron-energy-loss spectra and the structural stability of nickel oxide: An LSDA+U study, *Phys. Rev. B: Condens. Matter Mater. Phys.*, 1998, **57**, 1505.

31 L. Wang, T. Maxisch and G. Ceder, Oxidation energies of transition metal oxides within the GGA + U framework, *Phys. Rev. B: Condens. Matter Mater. Phys.*, 2006, **73**, 195107.

32 M. Cococcioni and S. de Gironcoli, Linear response approach to the calculation of the effective interaction parameters in the *LDA + U* method, *Phys. Rev. B: Condens. Matter Mater. Phys.*, 2005, **71**, 035105.

33 G. Henkelman, B. P. Uberuaga and H. Jónsson, A climbing image nudged elastic band method for finding saddle points and minimum energy paths, *J. Chem. Phys.*, 2000, **113**, 9901.

34 D. Sheppard, P. Xiao, W. Chemelewski, D. D. Johnson and G. Henkelman, A generalized solid-state nudged elastic band method, *J. Chem. Phys.*, 2012, **136**, 074103.

35 P. G. Dacosta, O. H. Nielsen and K. Kunc, Stress theorem in the determination of static equilibrium by the density functional method, *J. Phys. C: Solid State Phys.*, 1986, **19**, 3163.

This journal is © The Royal Society of Chemistry 2025

J. Mater. Chem. A, 2025, **13**, 30661–30668 | **30667**

36 G. P. Francis and M. C. Payne, Finite basis set corrections to total energy pseudopotential calculations, *J. Phys.: Condens. Matter*, 1990, **2**, 4395.

37 D. S. Lambert and D. D. O'Regan, Use of *DFT + U + J* with linear response parameters to predict non-magnetic oxide band gaps with hybrid-functional accuracy, *Phys. Rev. Res.*, 2023, **5**, 013160.

38 G. C. Moore, M. K. Horton, E. Linscott, A. M. Ganose, M. Siron, D. D. O'Regan and K. A. Persson, High-throughput determination of Hubbard *U* and Hund *J* values for transition metal oxides via the linear response formalism, *Phys. Rev. Mater.*, 2024, **8**, 014409.

39 R. Tesch and P. M. Kowalski, Hubbard *U* parameters for transition metals from first principles, *Phys. Rev. B*, 2022, **105**, 195153.

40 Q. Zhao, E. I. Ioannidis and H. J. Kulik, Global and local curvature in density functional theory, *J. Chem. Phys.*, 2016, **145**, 054109.

41 B. Kolb and T. Thonhauser, van der Waals density functional study of energetic, structural, and vibrational properties of small water clusters and ice I$_h$, *Phys. Rev. B: Condens. Matter Mater. Phys.*, 2011, **84**, 045116.

42 K. Liu, J. D. Cruzan and R. J. Saykally, Water Clusters, *Science*, 1996, **271**, 929.

43 U. Bergmann, A. D. Cicco, P. Wernet, E. Principi, P. Glatzel and A. Nilsson, Nearest-neighbor oxygen distances in liquid water and ice observed by x-ray Raman based extended x-ray absorption fine structure, *J. Chem. Phys.*, 2007, **127**, 174504.

44 S. Ullah, K. Tan, D. Sensharma, N. Kumar, S. Mukherjee, A. A. Bezrukov, J. Li, M. J. Zaworotko and T. Thonhauser, CO$_2$ Capture by Hybrid Ultramicroporous TIFSIX-3-Ni under Humid Conditions Using Non-Equilibrium Cycling, *Angew. Chem., Int. Ed.*, 2022, **61**, e202206613.

45 A. Edwards, L. J. Elkins, C. Slebodnick, J. Wang, Q. Zhang and T. A. Makal, Structural diversity and solvent-induced transformations of a copper-based metal-organic framework with highly aromatic ligands, *Dalton Trans.*, 2024, **53**, 14496.

46 J. Pang, M. Wu, J.-S. Qin, C. Liu, C. T. Lollar, D. Yuan, M. Hong and H.-C. Zhou, Solvent-Assisted, Thermally Triggered Structural Transformation in Flexible Mesoporous Metal-Organic Frameworks, *Chem. Mater.*, 2019, **31**, 8787.

47 E. Chapman, S. Ullah, H. Wang, L. Feng, K. Wang, H.-C. Zhou, J. Li, T. Thonhauser and K. Tan, Tuning the Adsorption Properties of Metal-Organic Frameworks through Coadsorbed Ammonia, *ACS Appl. Mater. Interfaces*, 2021, **13**, 43661.

48 A. Luna-Triguero, E. Andres-Garcia, P. Leo, W. Rook and F. Kapteijn, Guest-induced structural deformation in Cu-based metal-organic framework upon hydrocarbon adsorption, *Microporous Mesoporous Mater.*, 2023, **360**, 112699.

49 F.-X. Coudert, M. Jeffroy, A. H. Fuchs, A. Boutin and C. Mellot-Draznieks, Thermodynamics of Guest-Induced Structural Transitions in Hybrid Organic-Inorganic Frameworks, *J. Am. Chem. Soc.*, 2008, **130**, 14294.

50 K. Tan, S. Zuluaga, E. Fuentes, E. C. Mattson, J.-F. Veyan, H. Wang, J. Li, T. Thonhauser and Y. J. Chabal, Trapping gases in metal-organic frameworks with a selective surface molecular barrier layer, *Nat. Commun.*, 2016, **7**, 13871.

30668 | *J. Mater. Chem. A*, 2025, **13**, 30661–30668

This journal is © The Royal Society of Chemistry 2025